Journal of Materials Chemistry A

Accepted Manuscript

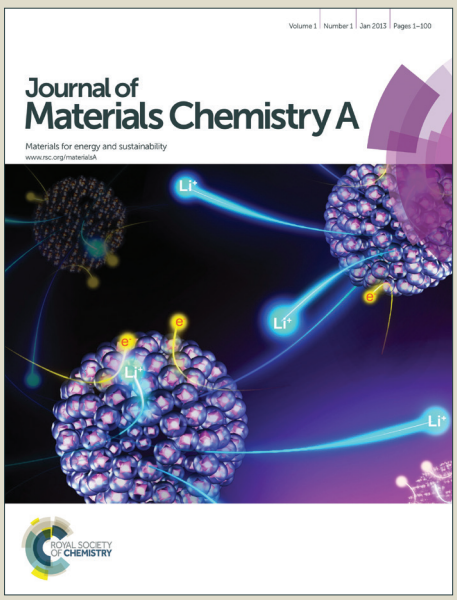

ROYAL SOCIETY OF CHEMISTRY

www.rsc.org/materialsA

Cite this: DOI: 10.1039/c0xx00000x

www.rsc.org/xxxxxx

ARTICLE TYPE

Graphene-like MoS_2/graphene Nanocomposite as High-performance Anode for Lithium Ion Batteries

Yongchang Liu, Yanping Zhao, Lifang Jiao* and Jun Chen

Received (in XXX, XXX) Xth XXXXXXXXX 20XX, Accepted Xth XXXXXXXXX 20XX

DOI: 10.1039/b000000x

In this article, we report on the preparation of graphene-like MoS_2/graphene nanocomposite by the hydrolysis of lithiated MoS_2 ($LiMoS_2$) and its application as anode material of lithium ion batteries. When the mass ratio of graphene/$LiMoS_2$ is 15/100, the obtained composite (MoS_2/GNS-15) displays a flower-like architecture composed of exfoliated nanosheets. The structure analyses further demonstrate that graphene-like MoS_2 is supported on the surface of graphene nanosheets (GNS), and some of the interlayer spacings of MoS_2 are enlarged with the intercalation of graphene. The reversible capacity of MoS_2/GNS-15 nanocomposite exhibits ~1400 mA h g^{-1} in the initial cycle and maintains 1351 mA h g^{-1} after 200 cycles at 100 mA g^{-1}. Furthermore, the capacity can reach 591 mA h g^{-1} even at a high current density of 1000 mA g^{-1}. The excellent electrochemical performance of MoS_2/GNS-15 is owing to the synergetic effect between high conductive GNS and graphene-like MoS_2. On one hand, GNS matrix can offer two-dimensional conductive networks and effectively suppress the aggregation of layered MoS_2 during lithiation/delithiation process. On the other hand, graphene-like MoS_2 with enlarged gallery can ensure the flooding of electrolyte, provide more active sites and lower the diffusion energy barrier of Li^+ ions.

Introduction

Lithium ion batteries (LIBs) have been widely used in electronic devices including cell phones, laptop computers and power tools.[1] However, the commercialized graphite as the anode material still suffers from a relatively low capacity (372 mA h g^{-1}).[2] Graphene with a monolayer graphite, which exhibits outstanding electronic behavior, large surface area and high chemical tolerance, has been applied to a wide range of fields.[3,4] For example, graphene nanosheets (GNS) and their composites have been intensively investigated as alternative anode marerials for LIBs with higher capacities.[5,6]

The versatility and success of graphene also stimulate the research interest into other two-dimensional inorganic nanosheets such as transition metal dichalcogenides (TMDs).[7] As a typical member of layered TMDs, MoS_2 has a sandwich structure that consists of covalently bond S-Mo-S trilayers separated by a relatively large van der Waals interaction.[8] MoS_2 shows versatile applications in the areas of lubricant, catalytic hydrodesulfuration, hydrogen storage or evolution reactions,[9-12] and can be used as a host for reversible insertion/extraction of Li^+/Mg^{2+}.[13-15] When the first lithium ion battery patent with MoS_2 as the anode material was granted in 1980,[16] a number of different morphologies of MoS_2 (including nanoflake, nanoflower, hierarchical sphere, *etc.*) used in LIBs were subsequently observed.[17-19] The specific capacity could be up to 1000 mA h g^{-1}, but their cycling stability was unsatisfactory. Researches show that carbon is a commonly used conductive additive in electrode materials, the structure of which is stable upon long cycling.[20,21] Hence the design of composite anodes based on carbonaceous materials is a promising strategy for improving the cyclability.[22,23] More specifically, recent studies have demonstrated that combining GNS with MoS_2 is a good choice to achieve considerable capacity as well as superior cycling stability, owing to the high electronic conductivity and synergistic effect between the components of the composites.[24] As an example, the capacity of MoS_2/GNS composite can reach 1300 mA h g^{-1} at 100 mA g^{-1} with tiny fading for 50 cycles.[25]

The similarity of layered structure between graphite and MoS_2 indicates that MoS_2 can be exfoliated to single-layer or few-layer sheets (named graphene-like structure).[26] Indeed, it has been shown that the transition metal disulfide nanosheets with few-layer (in particular single-layer) show distinctively different physical and chemical properties in comparison with the bulk counterparts.[27-29] When used as electrode materials of LIBs, the exfoliated MoS_2 display open channels for ion diffusion and provide more active sites, thus exhibiting improved electrochemical performance.[30-33]

Motivated by the above considerations, in this paper, we synthesized a novel kind of graphene-like MoS_2/GNS nanocomposite by the hydrolysis of lithiated MoS_2. Instrumental characterizations demonstrate that exfoliated MoS_2 is supported on the graphene substrate, meanwhile, some of the interlayer spacings of MoS_2 are enlarged with the intercalation of graphene.

It was found that the MoS_2/GNS nanocomposite exhibited excellent electrochemical performance in lithium ion batteries, delivering a high reversible capacity of 1300-1400 mA h g^{-1} with good cycling stability at 100 mA g^{-1}.

Experimental section

Synthesis of graphene nanosheets (GNS)

Graphene oxide (GO) was synthesized by the chemical oxidation of graphite flakes (Sigma-Aldrich) by a modified Hummers method.[34,35] The as-prepared GO was then reduced by thermal exfoliation at 800 °C in a quartz tube under Ar-H_2 (9:1 v/v) flow for 30 min to form fluffy GNS (the morphology of as-prepared GNS see ESI, Fig. S1†).

Synthesis of graphene-like MoS_2/GNS nanocomposite

In a typical synthesis, commercial bulk MoS_2 (J&K) was soaked in 2 equivalents butylithium (J&K, *n*-BuLi, 2.4 M in hexane) and kept in argon atmosphere for a week at room temperature. The concentration of *n*-Buli was adjusted to 1 M with the addition of anhydrous pentane before reaction. The product was filtered off in the dry box, washed with pentane and then dried under reduced pressure. The product stoichiometry is known to be $LiMoS_2$. Sonication of 100 mg $LiMoS_2$ with 15 mL deionized water resulted in the formation of single layers of MoS_2. The released hydrogen flow was speculated to push the adjacent MoS_2 layers further apart. The reactions are described as follows:[30]

$$MoS_2 + n\text{-BuLi} \rightarrow LiMoS_2 + 1/2C_8H_{18} \cdots\cdots\cdots\cdots (1)$$

$$LiMoS_2 + H_2O \rightarrow (MoS_2)_{\text{exfoliated layers}} + LiOH + 1/2H_2 \cdots\cdots (2)$$

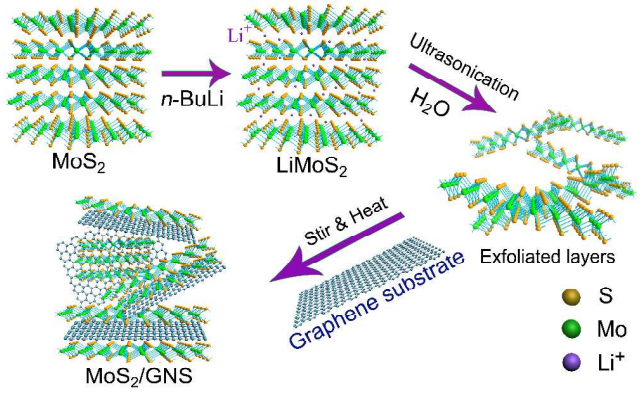

Scheme 1 Schematic formation process of MoS_2/GNS nanocomposite.

Then, the as-synthesized GNS was fully exfoliated and dispersed in ethanol with the help of ultrasonication (GNS/ethanol = 3 mg/mL). The GNS suspention was slowly added to the MoS_2 monolayers, the reaction mixture was kept sonication for 2h and then allowed to stir at room temperature for 4 days. The functional oxygen-containing groups on the surface of GNS could stretch into the positively charged area of MoS_2 molecule through electrostatic interaction. Hence the exfoliated graphene and MoS_2 would attach with each other during this process. Thereafter, two drops of concentrated hydrochloric acid were added, and the reaction mixture was allowed to stir in an airtight flask for another day at 80 °C. The single layers of MoS_2 were very sensitive to temperature and would restack turbostratically on the surface of GNS when heating.[30] In the meantime, some of the graphene would also be clamped between the restacked MoS_2 layers. The resultant black flocculations were collected by centrifugation with deionized water and ethanol for several times, and then dried in a vacuum oven at 80 °C for 12 h. The mass ratio of GNS/$LiMoS_2$ is 15/100 or 30/100, and the corresponding product is denoted as MoS_2/GNS-15 or MoS_2/GNS-30. As a control the restacked MoS_2 without any GNS was also fabricated. The preparation procedure for graphene-like MoS_2/GNS nanocomposite is illustrated in Scheme 1.

Materials Characterizations

X-Ray diffraction (XRD) analysis was performed on a Rigaku D/Max-2500 with Cu-Kα radiation (λ= 1.54178 Å). The morphology and microstructure were observed by scanning electron microscopy (SEM, HITACHI S-4800) and transmission electron microscopy (Tecnai G2 F20 TEM). The element content of the samples was analyzed by GENENIS-4000 energy dispersive X-Ray spectroscopy (EDX). Fourier transform infrared (FT-IR) spectra of the samples were collected at room temperature by using a FTIR-650 spectrometer (Tianjin Gangdong) at a resolution of 4 cm^{-1}. Raman spectrum (Renishaw inVia, excitation 514.5 nm) and X-ray photoelectron spectrometer (XPS, PHI 5000 Versaprobe, ULVAC PHI) were also used to characterize the synthesized materials.

Electrochemical Measurements

Electrochemical tests were carried out using a two-electrode cell assembled in an argon-filled glove box with water and oxygen contents below 5 ppm. The working electrodes were fabricated by mixing active materials, acetylene black and polyvinylidene fluoride (PVDF) binder with a weight ratio of 80:15:5 in N-methyl-pyrrolidinone (NMP) solvent to form homogeneous slurry. The mixture was coated on a Cu foil. The coated electrode was dried at 60 °C for 12 h in vacuum oven and then pressed. The active material loading was about 0.9-1.0 mg cm^{-2} after wiping off the mass of graphene. The counter/reference electrode was lithium metal and the electrolyte solution was 1 M $LiPF_6$ in a volume ratio of 1:1:1 mixture of ethylene carbonate (EC), ethylene methyl carbonate (EMC) and dimethyl carbonate (DMC). The separator was Celgard 2320 microporous film. Galvanostatic charge/discharge tests were performed between 0.01 and 3.0 V on a LAND battery-test instrument (CT2001A). Cyclic voltammetries (the potential interval: 0.01-3.0 V) were conducted by a CHI660B electrochemical workstation at a scan rate of 0.2 mV s^{-1}.

Results and discussion

Fig. 1 shows the XRD patterns of bulk MoS_2, pure restacked MoS_2, the MoS_2/GNS-15 and MoS_2/GNS-30 nanocomposites. All the sharp diffraction peaks of bulk MoS_2 can be readily indexed to a hexagonal phase (JCPDS No. 37-1492). The strong (002) peak with a *d*-spacing of 0.62 nm signifies a well-stacked layered structure along the *c* axis.[24] In comparison, restacked MoS_2 shows broadened peaks and a much shortened (002) peak. This indicates that the mean crystallite size and the number of layers along the *c* axis are much smaller than those of raw MoS_2 (from

over 70 layers to about 9-10 layers, extracted from the full width at half maximum (FWHM)).[30,36] Additionally, the MoS_2/GNS composites basically retain the position of the diffraction peaks of MoS_2, while the intensity becomes even weaker. This implies that the incorporation of GNS further restrains the stacking of MoS_2 layers. Moreover, we can hardly detect the (002) diffraction peak of graphene at $2\theta \approx 25°$, denoting that the graphene nanosheets seldom stack together. It may be attributed to the layered MoS_2, which is anchored on the surface of graphene and inhibits the stacking of GNS. Meanwhile, two new peaks assigned to (001) and (003) planes appear more and more obvious with increasing graphene proportion in the composites. This suggests that some of the graphene is lying in the van der Walls gap of host MoS_2, leading to an expansion of the interplanar spacing.[36,37]

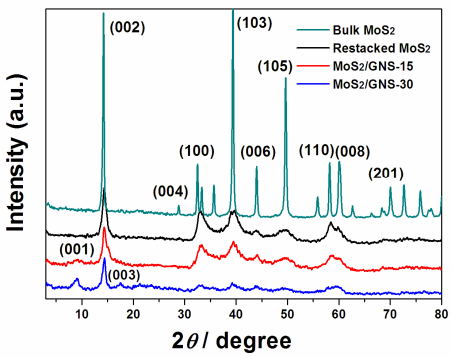

Fig. 1 XRD patterns of bulk MoS_2, pure restacked MoS_2, MoS_2/GNS-15 and MoS_2/GNS-30 nanocomposites.

Fig. 2 shows the SEM and HRTEM images of the bulk MoS_2 and MoS_2/GNS-15 nanocomposite. The building blocks of bulk MoS_2 are largely micrometer-sized inerratic nanosheets, which are tightly stacked (Fig. 2a). After exfoliation, the morphology of restacked MoS_2 interestingly changed to highly-scattered nanoflakes (see ESI, Fig. S2a†). It is also noted that the size and thickness of the nanosheets were significantly decreased relative to bulk phase. This confirms the fact that restacked MoS_2 has the structure of a single layer or few layers, which was named graphene-like structure by Rao *et al*.[38] Introducing optimum level of GNS is responsible for an order arrangement of the graphene-like nanoflakes, probably due to the flexible graphene which acts as a substrate for layered MoS_2, would self-assemble into a 3D architecture by partial overlapping or coalescing.[24] As shown in Fig. 2b, MoS_2/GNS-15 nanocomposite exhibits a flower-like architecture constituted by exfoliated nanosheets. However, excess GNS will inevitably block the open-framework structure of the composite. For MoS_2/GNS-30, the flower-like architecture is overlapped with large areas of graphene (see ESI, Fig. S2b†). HRTEM image displayed in Fig. 2c reveals that bulk MoS_2 is composed of tens of layers tightly stacked together. In contrast, Fig. 2d indicates that MoS_2/GNS-15 nanocomposite contains highly exfoliated MoS_2 single layer or few layers, which are supported on the surface of graphene. It's worth noticing that some of the interlayer distances of MoS_2 are enlarged (from 6.2Å to ~10Å) with the intercalation of graphene, which is complying with the XRD observation. From the TEM element mapping image shown in Fig. 2e, the uniform distribution of Mo, S, C elements within the nanosheets clarifies the hybrid structure of MoS_2/GNS-15. In general, graphene-like MoS_2 with enlarged gallery can effectively shorten the migration path of Li^+, provide more active sites and lower the diffusion energy barrier of Li^+ ions.[39-42] The incorporated GNS would also form an interconnected conducting network, which is very important for the less-conducting MoS_2 as electrode materials.[43]

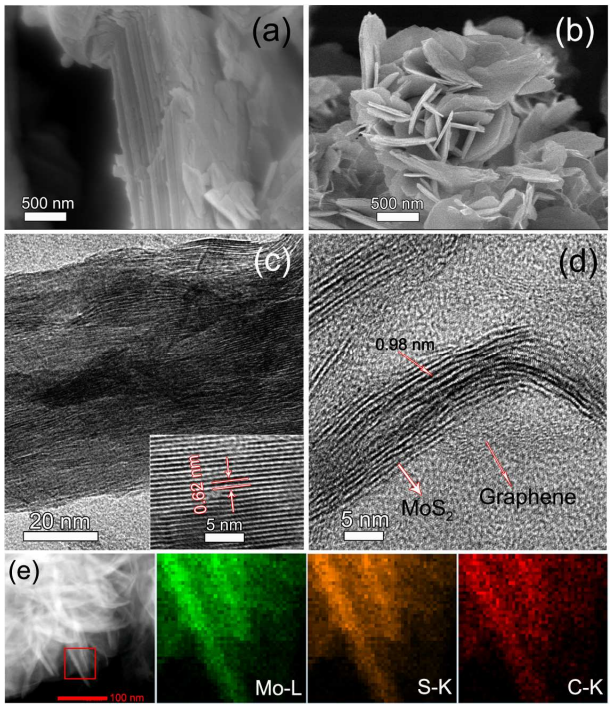

Fig. 2 SEM images of (a) bulk MoS_2, (b) MoS_2/GNS-15 nanocomposite; HRTEM images of (c) bulk MoS_2, (d) MoS_2/GNS-15 nanocomposite; (e) TEM element mapping image of MoS_2/GNS-15.

EDX analysis reveals that the MoS_2/GNS composites consist of C, Mo, S and a small number of O. The minimal oxygen element comes from the graphene oxide (GO), which is not reduced completely during the thermal exfoliation process. It is calculated that the atomic ratio of Mo to S approaches the theoretical value of MoS_2 (1:2), confirming the products to be stoichiometric MoS_2. The content of carbon is 13.9 wt.% and 24.1 wt.% in MoS_2/GNS-15 and MoS_2/GNS-30, respectively. In addition, the SEM EDX mapping of MoS_2/GNS-15 nanocomposite (see ESI, Fig. S3†) further demonstrates that MoS_2 are homogeneously distributed on the graphene substrate.

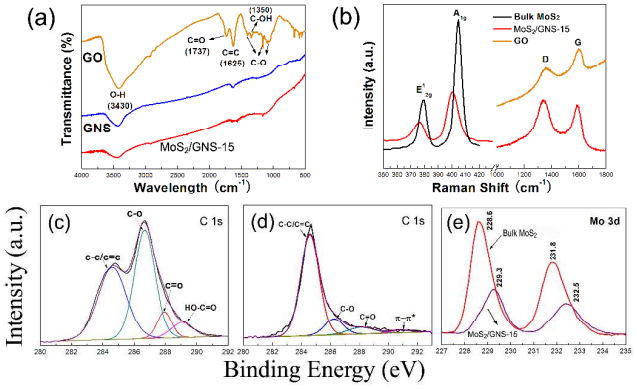

Fig. 3 (a) FT-IR spectra of as-prepared GO, GNS and MoS_2/GNS-15 nanocomposite; (b) Raman spectra of bulk MoS_2, MoS_2/GNS-15 and GO;

XPS spectra of (c) GO C1s; (d) MoS_2/GNS-15 C1s; (e) Mo3d of bulk MoS_2 and MoS_2/GNS-15.

Fourier transform infrared (FT-IR) spectra of the as-prepared GO, GNS and MoS_2/GNS-15 nanocomposite are displayed in Fig. 3a. The characteristic peaks of GO appear at around 1737 cm^{-1} (C=O), 1625 cm^{-1} (C=C), 1400 cm^{-1} (C-O), 1350 cm^{-1} (C-OH), 1150 cm^{-1} (C-O), and 1090 cm^{-1} (C-O), which are in accordance with previous literatures.[44] For GNS and MoS_2/GNS-15, these vibrations become much weaker and even hard to be detected, implying that the oxygen-containing groups have been largely removed.

Raman spectroscopy has been extensively used for the characterization of carbonaceous materials with different microstructures. Recently, it has also been used for the identification of single- and few-layer MoS_2 sheets.[45,46] Fig. 3b shows the Raman spectra of bulk MoS_2, MoS_2/GNS-15 and GO. The two dominant peaks of pristine MoS_2 at 379 and 405 cm^{-1} correspond to E^1_{2g} and A_{1g} modes of the hexagonal MoS_2, respectively. The E^1_{2g} mode involves the in-layer displacement of Mo and S atoms, whereas the A_{1g} mode involves the out-of-layer symmetric displacements of S atoms along the *c* axis.[47] By contrast, for MoS_2/GNS-15, the blue shift of A_{1g} and the decrease of the inter-peak separation between E^1_{2g} and A_{1g} are particular significant for the decreasing number of MoS_2 layers.[41] The A_{1g} peak at 401 cm^{-1} also exactly confirms the existence of single-layer MoS_2.[48] Additionally, the two modes become broader than those of bulk MoS_2, resulting from the phonon confinement of graphene-like structure.[28] Moreover, two other Raman peaks at 1350 and 1600 cm^{-1} can be seen in the spectrum of MoS_2/GNS-15, which are related very well to the D and G bands of graphene. In general, the D band is attributed to defects and disorder in the hexagonal graphic layers, while the G band is ascribed to the vibration of sp^2 carbon atoms in a 2D hexagonal lattice. The relative intensity ratio I_D/I_G is therefore an indication of the graphene quality. The calculated I_D/I_G value of the composite has been much increased as compared with that of GO, further proving the formation of exfoliated GNS with some defects and disordered structures.[48]

The degree of GO to GNS conversion can also be verified by the XPS spectra. In brief, the C1s XPS peak-fitting result of GO (Fig. 3c) clearly reveals a considerable degree of oxidation with four resolved peaks, corresponding to sp^2-hydridized C-C/C=C and oxygenated functional groups (C-O, C=O and O-C=O). While the C1s peak-fitting result of MoS_2/GNS-15 only exhibits C-C/C=C, C-O, C=O peaks and a π-π* peak, and the relative peak areas of C-O and C=O are much smaller relative to GO. Together with the disappearance of O-C=O peak, it confirms that a reduction process of GO occurred. In Fig. 3d, the Mo3d spectrum of bulk MoS_2 shows two peaks at 228.6 and 231.8 eV, which are attributed to the doublet $Mo3d_{5/2}$ and $Mo3d_{3/2}$ of Mo^{4+}. While the two peaks of the composite shift to 229.3 and 232.5 eV, respectively, the binding energy has increased by 0.7 eV. It is well known that binding energy increases with the improvement of electronegativity.[47] This result implies that the electronegativity around Mo element of MoS_2/GNS-15 is stronger than that of bulk MoS_2. This can be ascribed to the electrostatic interaction between tetravalent molybdenum and GNS, suggesting that the MoS_2/GNS nanocomposite is not simple physical mixture. Additionally, no peaks of elements other than Mo, S, C, O are observed in the survey XPS spectrum of MoS_2/GNS-15 (see ESI, Fig. S4†). The atomic ratio of Mo/S is approximately 1:2, which further manifests the high purity of MoS_2.

Next, we investigate the electrochemical properties of MoS_2/GNS composite as anode materials for LIBs. Fig. 4a shows the representative cyclic voltammograms (CVs) of MoS_2/GNS-15 electrode. This CV behavior is generally consistent with those reported previously.[13,24,25] In the first cathodic sweep, the peak at 0.85 V is attributed to the intercalation of lithium ions into the MoS_2 lattice which transforms the triangular prism (coordination of Mo by six S atoms) into an octahedral structure. The other peak at 0.2 V is assigned to the complete reduction process:

$$MoS_2 + 4Li \leftrightarrow Mo + 2Li_2S$$

In the following cathodic sweeps, two new peaks at 1.8 V and 1.0 V appear, perhaps suggesting the presence of a multi-step lithium insertion mechanism.[31,49] But the peak at 0.2 V is probably concealed by the overlap of electrochemical lithium storage in both MoS_2 and GNS.[48] In the anodic sweeps, only one peak at 2.4 V is observed, corresponding to the lithium extraction process and the oxidation of Mo to MoS_2.[49,50] Fig. 4b displays the first three charge-discharge voltage profiles of MoS_2/GNS-15 at a current density of 100 mA g^{-1}. In agreement with the above CV study, two plateaus at 1.1 V and 0.6 V are observed in the first discharge process. The first plateau at 1.1 V is attributed to the formation of Li_xMoS_2, and the plateau at 0.6 V corresponds to the conversion reaction process, in which Li_xMoS_2 is completely decomposed into Mo nanoparticles embedded in a Li_2S matrix. In the meantime, a gel-like polymeric layer is formed resulting from electrochemically driven electrolyte degradation. In the second and third discharge curves, MoS_2/GNS-15 electrode exhibits two potential plateaus at 1.9 V and 1.2 V, while the potential plateau at 0.6 V in the first discharge disappears. During the charge (delithiation) process, MoS_2/GNS-15 shows a conspicuous potential plateau at 2.4 V, which also agrees with the previous CV curves. In addition, during the first charge/discharge process, the lithiation capacity is 1779.8 mA h g^{-1}, and the delithiation capacity reaches 1398.7 mA h g^{-1}. It is worth noticing that from the second cycle, the discharge and charge curves are well overlapped, indicating the high reversibility and high capacity retention of MoS_2/GNS-15 electrode.

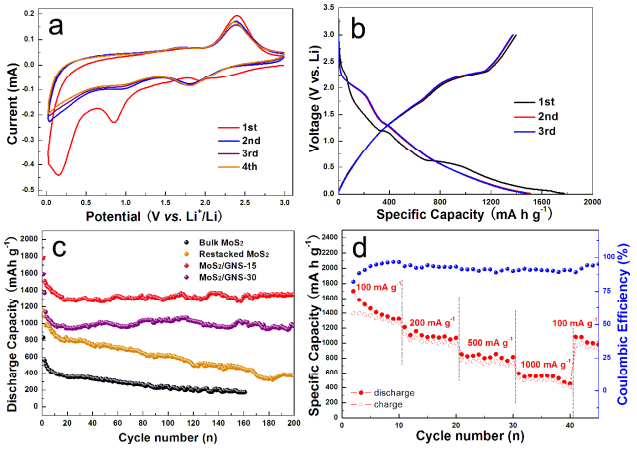

Fig. 4 Electrochemical performance: (a) cyclic voltammograms of MoS_2/GNS-15 electrode at a scanning rate of 0.2 mV s^{-1} during the first four cycles; (b) first three galvanostatic charge-discharge profiles of MoS_2/GNS-15; (c) cycling behaviors of the synthesized samples: bulk MoS_2, restacked MoS_2, MoS_2/GNS-15 and MoS_2/GNS-30; (d) rate capability and coulombic efficiency of MoS_2/GNS-15 electrode.

Fig. 4c shows the cycling performance of the as-synthesized samples evaluated at a discharge current density of 100 mA g^{-1}. The bulk MoS_2 electrode delivers a diminishing discharge capacity from over 500 mA h g^{-1} during initial cycles to 170.9 mA h g^{-1} at the 160th cycle (with the capacity retention of 33.2 %). After exfoliation, the restacked MoS_2 shows a much higher capacity of more than 900 mA h g^{-1}, but the cyclic stability is still poor, which can only sustain 365.1 mA h g^{-1} after 200 cycles (with the capacity retention of 37.4 %). When incorporating GNS on this basis, the discharge capacity and cyclic stability of MoS_2/GNS composites have been largely enhanced. It is remarkable that MoS_2/GNS-15 electrode displays an extraordinary capacity of 1483 mA h g^{-1} in the initial few cycles, and the capacity can still maintain 1351.2 mA h g^{-1} in the 200th cycle (with a capacity retention of 91.1 %). The capacity of MoS_2/GNS-30 is not as high as that of MoS_2/GNS-15, probably because too much graphene will significantly block the channels for Li^+ ion diffusion. But the excellent cycling stability is retained. The continuous capacity fading of all electrodes during the initial cycles is due to the side reactions of the electrodes with electrolyte, resulting in a large amount of irreversible trapped lithium. What's worth mentioning is that the achieved capacity and cyclability of MoS_2/GNS-15 are higher than most previously reported MoS_2-based anodes.[19,31,37] For example, at the same or lower current density, exfoliated MoS_2/PEO nanocomposite,[39] MoS_2/PANI nanowires and MoS_2/GNS composite were prepared as electrode materials for LIBs,[25,50] the corresponding capacities obtained were ~1100 mA h g^{-1}, 952.6 mA h g^{-1} and 1290 mA h g^{-1} after 50 cylces, respectively. We believe that the graphene-like MoS_2 supported on the high conductive graphene would increase the contact area with electrolyte, provide more reaction sites and facilitate the transportation of Li^+ ions, thus contributing to the great electrochemical performance of MoS_2/GNS-15. Fig. 4d further depicts the rate capability and coulombic efficiency of MoS_2/GNS-15, it can be seen that the composite also demonstrates good rate performance with a high coulombic efficiency (near 95%). Even at a high current density of 1000 mA g^{-1}, the capacity remains at 591 mA h g^{-1}, which is still higher than that of bulk MoS_2 or free GNS (see ESI, Fig. S5†).

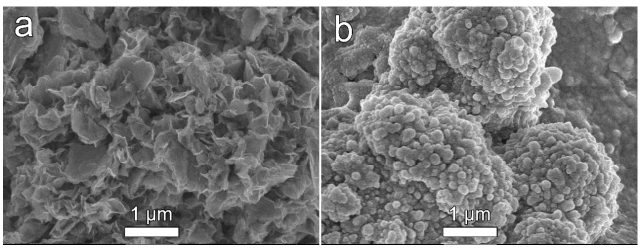

Fig. 5 SEM images of (a) MoS_2/GNS-15 electrode and (b) restacked MoS_2 electrode after been discharged/charged for 200 cycles at 100 mA g^{-1}.

Moreover, the morphology changes of the representative electrodes after discharge/charge cycles were checked by SEM. Fig. 5a shows that MoS_2/GNS-15 nanocomposite still sustains the flower-like architecture after 200 cycles at 100 mA g^{-1}. Though MoS_2 would decompose during cycling, the GNS substrate could effectively inhibit the aggregation of the generated Mo nanoparticles and amorphous Li_2S. In addition, the two-dimensional graphene lay in MoS_2 gallery could act as a support framework, which is also beneficial for the preservation of layered structure. The graphene-like structure with large specific surface area can continuously keep the accessibility of the Li^+ host, as well as the high utilization rate of active materials. On the contrary, as displayed in Fig. 5b, the original lamellar restacked MoS_2 changes to big solid bulks agglomerated by lots of small particles. Such a structure is bound to hinder the infiltration of electrolyte and the insertion-extraction kinetics of Li^+. So it is not difficult to understand the poor cycling stability of restacked MoS_2.

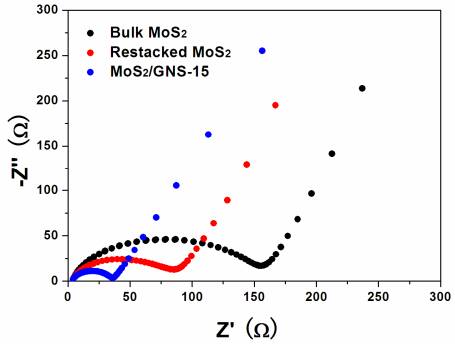

Fig. 6 Electrochemical impedance spectra of the bulk MoS_2, restacked MoS_2, MoS_2/GNS-15 electrodes.

The electrochemical impedance spectra (EIS) of bulk MoS_2, restacked MoS_2 and MoS_2/GNS-15 electrodes are compared in Fig. 6. The resistance of restacked MoS_2 is much lower than that of bulk MoS_2, implying graphene-lke structure can facilitate the transportation of Li^+ ions. Furthermore, the even lower impedance of MoS_2/GNS-15 confirms that the incorporation of graphene effectively enhances the conductivity of MoS_2. The excellent electrochemical performance of MoS_2/GNS-15 for reversible Li^+ storage can be ascribed to the synergetic effect between high conductive GNS and graphene-like MoS_2. An interpretation follows. First, the incorporation of GNS matrix not only offers two-dimensional conductive networks and effective buffering for volume expansion, but also avoids the aggregation of layered MoS_2 during lithiation/delithiation process.[51] These are helpful for high cycling stability. Second, the specific graphene-like MoS_2 with enlarged interlayer spacing is readily accessible to the electrolyte, and can facilitate the reversible Li^+ insertion-extraction kinetics, thus increasing the utilization rate of active materials.

Conclusions

In summary, graphene-like MoS_2/graphene nanocomposite was successfully fabricated by a lithiation-assisted exfoliation method. When the mass ratio of GNS/$LiMoS_2$ is 15/100, the obtained MoS_2/GNS-15 displays a flower-like architecture constituted by exfoliated nanosheets. Instrumental characterizations demonstrate that the graphene-like MoS_2 is

supported on the surface of GNS, and some of the interlayer spacings of MoS_2 are enlarged with the intercalation of graphene. When used as anode for lithium ion batteries, MoS_2/GNS-15 nanocomposite exhibits much higher specific capacity as well as superior cycling performance than bulk MoS_2. It can deliver an extraordinary reversible capacity of ~1400 mA h g^{-1} in the initial cycle and sustain 1351 mA h g^{-1} after 200 cycles at 100 mA g^{-1}. Therefore, the present results turn out that this novel MoS_2/GNS nanocomposite hold promise as anode materials for high-performance LIBs.

Acknowledgements

This work was financially supported by the programs of National 973 (2011CB935900), NSFC (51231003) and MOE (B12015, 113016A and IRT-13R30).

Notes and references

Key Laboratory of Advanced Energy Materials Chemistry (MOE), College of Chemistry, Collaborative Innovation Center of Chemical Science and Engineering, Nankai University, Tianjin 300071, P.R. China, Tel.: +86 22 23504527; fax: +86 22 23509571; E-mail: jiaolf@nankai.edu.cn.

†Electronic Supplementary Information (ESI) available: [Fig. S1-S5]. See DOI: 10.1039/b000000x/

1 C. F. Zhang, Z. X. Chen, Z. P. Guo and X. W. Lou, *Energy Environ. Sci.*, 2013, **6**, 974.
2 E. Yoo, J. Kim, E. Hosono, H. Zhou, T. Kudo and I. Honma, *Nano Lett.*, 2008, **8**, 2277.
3 K. S. Novoselov, A. K. Geim, S. V. Morozov, D. Jiang, Y. Zhang, S. V. Dubonos, I. V. Grigorieva and A. A. Firsov, *Science*, 2004, **306**, 666.
4 X. Huang, Z. Yin, S. Wu, X. Qi, Q. He, Q. Zhang, Q. Yan, F. Boey and H. Zhang, *Small*, 2011, **7**, 1876.
5 G. X. Wang, X. P. Shen, J. Yao and J. Park, *Carbon*, 2009, **47**, 2049.
6 B. Ding, C. Z. Yuan, L. F. Shen, G. Y. Xu, P. Nie, Q. X. Lai and X. G. Zhang, *J. Mater. Chem. A*, 2013, **1**, 1096.
7 M. Chhowalla, H. S. Shin, G. Eda, L. J. Li, K. P. Loh and H. Zhang, *Nat. Chem.*, 2013, **5**, 263.
8 G. Eda, T. Fujita, H. Yamaguchi, D. Voiry, M. W. Chen and M. Chhowalla, *ACS Nano*, 2012, **6**, 7311.
9 M. Chhowalla and G. A. Amaratunga, *Nature*, 2000, **407**, 164.
10 J. Chen, N. Kuriyama, H. T. Yuan, H. T. Takeshita and T. Sakai, *J. Am. Chem. Soc.*, 2001, **123**, 11813.
11 F. Y. Cheng, J. Chen and X. L. Gou, *Adv. Mater.*, 2006, **18**, 2561.
12 D. Merki and X. L. Hu, *Energy Environ. Sci.*, 2011, **4**, 3878.
13 S. J. Ding, J. S. Chen and X. W. Lou, *Chem. -Eur. J.*, 2011, **17**, 13142.
14 Y. L. Liang, R. J. Feng, S. Q. Yang, H. Ma, J. Liang and J. Chen, *Adv. Mater.*, 2011, **23**, 640.
15 Y. C. Liu, L. F. Jiao, Q. Wu, J. Du, Y. P. Zhao, Y. C. Si, Y. J. Wang and H. T. Yuan, *J. Mater. Chem. A*, 2013, **1**, 5822.
16 R. R. Haering, J. A. R. Stiles and K. Brandt, US Patent 4224390, 1980.
17 C. Q. Feng, J. Ma, H. Li, R. Zeng, Z. P. Guo and H. K. Liu, *Mater. Res. Bull.*, 2009, **44**, 1811.
18 M. Wang, G. D. Li, H. Y. Xu, Y. T. Qian and J. Yang, *ACS Appl. Mater. Interfaces*, 2013, **5**, 1003.
19 T. Stephenson, Z. Li, B. Olsen and D. Mitlin, *Energy Environ. Sci.*, 2014, **7**, 209.
20 M. Gu, Y. Li, X. L. Li, S. Y. Hu, X. W. Zhang, W. Xu, S. Thevuthasan, D. R. Baer, J. G. Zhang, J. Liu and C. M. Wang, *ACS Nano*, 2012, **6**, 8439.
21 L. W. Ji, M. Gu, Y. Y. Shao, X. L. Li, M. H. Engelhard, B. W. Arey, W. Wang, Z. M. Nie, J. Xiao, C. M. Wang, J. G. Zhang and J. Liu, *Adv. Mater.*, 2014, **26**, 2901.
22 J. Lin, Z. W. Peng, C. S. Xiang, G. D. Ruan, Z. Yan, D. Natelson and J. M. Tour, *ACS Nano*, 2013, **7**, 6001.
23 J. M. Zheng, M .Gu, M. J. Wagner, K. A. Hays, X. H. Li, P. J. Zuo, C. M. Wang, J. G. Zhang, J. Liu and J. Xiao, *J. Electrochem. Soc*. 2013, **160**, A1624.
24 K. Chang and W. X. Chen, *ACS Nano*, 2011, **5**, 4720.
25 K. Chang and W. X. Chen, *Chem. Commun.*, 2011, **47**, 4252.
26 M. S. Xu, T. Liang, M. M. Shi and H. Z. Chen, *Chem. Rev.*, 2013, **113**, 3766.
27 V. Nicolosi, M. Chhowalla, M. G. Kanatzidis, M. S. Strano and J. N. Coleman, *Science*, 2013, **340**, 1226419.
28 Z. Y. Zeng, Z. Y. Yin, X. Huang, H. Li, Q. Y. He, G. Lu, F. Boey and H. Zhang, *Angew. Chem. Int. Ed.*, 2011, **50**, 11093.
29 X. Huang, Z. Y. Zeng and H. Zhang, *Chem. Soc. Rev.*, 2013, **42**, 1934.
30 G. D. Du, Z. P. Guo, S. Q. Wang, R. Zeng, Z. X. Chen and H. K. Liu, *Chem. Commun.*, 2010, **46**, 1106.
31 J. Xiao, X. J. Wang, X. Q. Yang, S. D. Xun, G. Liu, P. K. Koech, J. Liu and P. Lemmon, *Adv. Funct. Mater.*, 2011, **21**, 2840.
32 V. H. Pham, K. H. Kim, D. W. Jung, K. Singh, E. S. Oh and J. S. Chung, *J. Power Sources*, 2013, **244**, 280.
33 H. Hwang, H. Kim and J. Cho, *Nano Lett.*, 2011, **11**, 4826.
34 W. S. Hummers and R. E. Offeman, *J. Am. Chem. Soc.*, 1958, **80**, 1339.
35 S. Zhang, Y. Shao, H. Liao, M. H. Engelhard, G. Yin and Y. Lin, *ACS Nano*, 2011, **5**, 1785.
36 B. E. Aharon, A. Albo, M. Kalina and G. L. Frey, *Adv. Funct. Mater.*, 2006, **16**, 980.
37 K. Chang, W. X. Chen, L. Ma, H. Li, He. Li, F. H. Huang, Z. D. Xu, Q. B. Zhang and J. Y. Lee, *J. Mater. Chem.*, 2011, **21**, 6251.
38 H. S. S. Ramakrishna Matte, A. Gomathi, A. K. Manna, D. J. Late, R. Datta, S. K. Pati, C. N. R. Rao, *Angew. Chem. Int. Ed.*, 2010, **49**, 4059.
39 J. Xiao, D. Choi, L. Cosimbescu, P. Koech, J. Liu and J. P. Lemmon, *Chem. Mater.*, 2010, **22**, 4522.
40 Y. G. Guo, J. S. Hu and L. J. Wan, *Adv. Mater.*, 2008, **20**, 2878.
41 A. Magasinski, P. Dixon, B. Hertxberg, A. Kvit, J. Ayala and G. Yushin, *Nat. Mater.*, 2010, **9**, 353.
42 Y. F. Li, D. H. Wu, Z. Zhou, C. R. Cabrera and Z. F. Chen, *J. Phys. Chem. Lett.*, 2012, **3**, 2221.
43 X. S. Zhou, L. J. Wan and Y. G. Guo, *Chem. Commun.*, 2013, **49**, 1838.
44 L. X. Lin and S. W. Zhang, *J. Mater. Chem.*, 2012, **22**, 14385.
45 G. Lee, H. G. Yan, L. E. Brus, T. F. Heinz, J. Hone and S. Ryu, *ACS Nano*, 2010, **4**, 2695.
46 Li, Q. Zhang, C. C. R. Yap, B. K. Tay, T. H. T. Edwin, A. Oliver and D. Baiwargeat, *Adv. Funct. Mater.*, 2012, **22**, 1385.
47 Y. C. Liu, L. F. Jiao, Q. Wu, Y. P. Zhao, K. Z. Cao, H. Q. Liu, Y. J. Wang and H. T. Yuan, *Nanoscale*, 2013, **5**. 9562.
48 Z. Wang, T. Chen, W. X. Chen, K. Chang, L. Ma, G. C. Huang, D. Y. Chen and J. Y. Lee, *J. Mater. Chem. A*, 2013, **1**, 2202.
49 S. J. Ding, D. Y. Zhang, J. S. Chen and X. W. Lou, *Nanoscale* **2012**, *4*, 95.
50 L. C. Yang, S. N. Wang, J. J. Mao, J. W. Deng, Q. S. Gao, Y. Tang and O. G. Schmidt, *Adv. Mater.*, 2013, **25**, 1180.
51 S. Stankovich, D. A. dikin, G. H. B. Dommett, K. M. Kohlhaas, E. J. Zimney, E. A. Stach, R. D. Piner, S. T. Nguyen and R. S. Ruoff, *Nature*, 2006, **442**, 282.